

Learning Position-Aware Implicit Neural Network for Real-World Face Inpainting

Bo Zhao¹, Huan Yang^{2*}, Jianlong Fu²

¹ Beijing Institute of Technology, ² Microsoft Research Asian
1198327714@qq.com, huayan@microsoft.com, jianf@microsoft.com

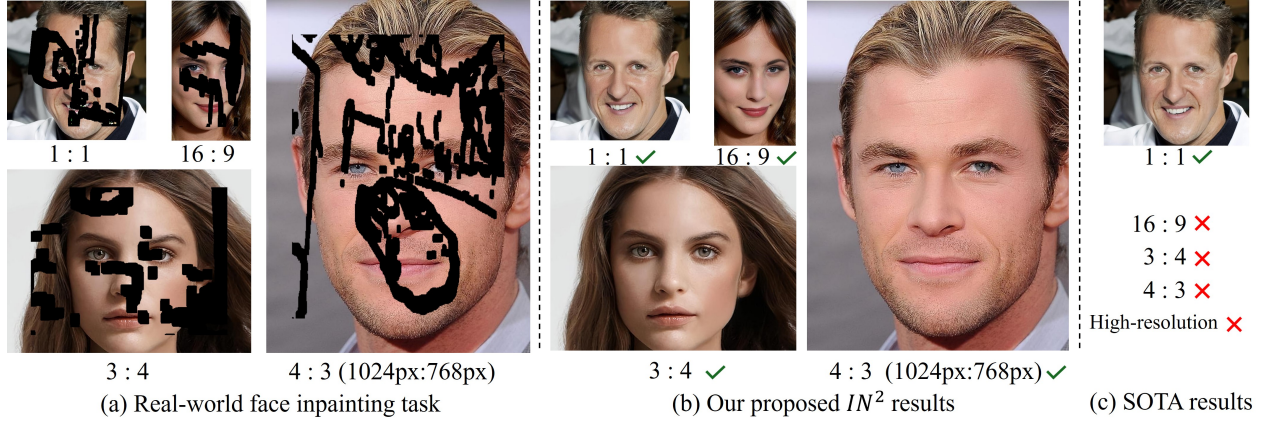


Figure 1: An illustration of real-world face inpainting scenarios and comparison between our proposed methods and SOTA approaches. (a) Examples of real-world inpainting images of different aspect ratios and resolutions. (b) Our proposed method can process the input of arbitrary resolution robustly (e.g., $1024px \times 768px$) at the fine structure, even trained around $512px \times 512px$. (c) Existing SOTA methods could only work well on images in 1:1 aspect ratio with the low-resolution format.

Abstract

Face inpainting requires the model to have a precise global understanding of the facial position structure. Benefiting from the powerful capabilities of deep learning backbones, recent works in face inpainting have achieved decent performance in ideal setting (square shape with $512px$). However, existing methods often produce a visually unpleasant result, especially in the position-sensitive details (e.g., eyes and nose), when directly applied to arbitrary-shaped images in real-world scenarios. The visually unpleasant position-sensitive details indicate the shortcomings of existing methods in terms of position information processing capability. In this paper, we propose an Implicit Neural Inpainting Network (IN^2) to handle arbitrary-shape face images in real-world scenarios by explicit modeling for position information. Specifically, a downsample processing encoder is proposed to reduce information loss while obtaining the global semantic feature. A neighbor hybrid attention block is proposed with a hybrid attention mechanism

to improve the facial understanding ability of the model without restricting the shape of the input. Finally, an implicit neural pyramid decoder is introduced to explicitly model position information and bridge the gap between low-resolution features and high-resolution output. Extensive experiments demonstrate the superiority of the proposed method in real-world face inpainting task.

1 Introduction

Image inpainting aims to generate plausible content to complete the missing regions. Compared to image inpainting which focuses more on extracting relevant information from unmasked backgrounds, face inpainting requires the model to have a global understanding of the facial position structure, which is more challenging. With the flourishing development of deep neural networks (DNNs) [Krizhevsky *et al.*, 2012] and generative adversarial networks (GANs) [Goodfellow *et al.*, 2014], face inpainting has made significant progress. Specifically, previous works focus on the generated content and now can produce more realistic texture [Xu *et al.*, 2021a] and diversified inpainting results [Li *et al.*, 2022] in ideal settings (e.g., $512px \times 512px$). However, the real-

* Corresponding author

world settings from downstream applications are quite different from the ideal setting, where arbitrary-size inputs are what we have to cope with. Compared to the content and texture of general scenes, the position-sensitive face structure information is more affected by changes in image shape, which makes face inpainting in real-world scenarios more challenging. When existing methods work in real-world scenarios, they can only accept specific inputs, as shown in Tab. 1.

More importantly, when the shape and size change, they tend to produce the results with misaligned eyes and nose, as shown in Fig. 2 (b). It indicates existing methods are unable to form a satisfactory understanding of the position-sensitive facial structure in real-world scenarios, which results in a performance drop, as shown in Tab. 2.

Different inference settings and retraining have been tried to adapt previous methods to arbitrary-size input. By mitigating the gap in spatial structure information between training data and testing data, resizing can simply and effectively improve the performance of the model in most scenarios. Although extra resize processing is adopted, the duplicate artifacts are serious in the position-sensitive areas, such as eyes and nose, shown in Fig. 2 (d), which indicates the ineffective position information modeling [Xu *et al.*, 2021b].

It is worth noticing that the arbitrary-shape image super-resolution (SR) task has been solved by representing an image with Implicit Neural Representation (INR). INR represents an object as a function that maps position to the corresponding signal value to model position information better [Chen *et al.*, 2021]. Compared with the SR task, face inpainting requires a larger receptive field for facial structure understanding to complete the masked areas. Therefore, how to leverage position information effectively to adapt the inpainting model to real-world face inpainting task is still an open problem.

In this paper, we develop a new INR inpainting model, capable of generating robust results for real-world face inpainting task due to its capacity to explicitly model position information. To deal with real-world high-resolution input, downsampling is an inevitable operation. Noticing the commonly used cascaded downsampling in the encoder may lead to information loss during the encoding process, we propose the **Downscale Processing Block (DPB)** to alleviate this problem. Although the popular window-based attention mechanism [Vaswani *et al.*, 2017] is beneficial for facial structure learning [Li *et al.*, 2022], it restricts the acceptable inputs, which is not conducive to its application in real-world scenarios. With neighborhood Attention [Hassani *et al.*, 2023], we propose a new variant of attention block to overcome this problem and learn better facial features, named **Neighbor Hybrid Attention Block (NHAB)**. Finally, we propose an **Implicit Neural Pyramid Decoder (INPD)** to model the position information explicitly and mitigate the gap between low-resolution feature to high-resolution output. Thanks to the previous design, our model can directly deal with inputs of arbitrary size. Therefore, we design an **Adaptation Training Strategy (ATS)** which randomly crops input to irregular shapes to improve the facial spatial structure modeling ability of the model for the real-world challenge. As shown in Fig. 1 (b), our method successfully restores arbitrary-shape input even in position-sensitive details. Our contributions are

summarized as:

- As far as we know, we are the first to propose the real-world face inpainting task from the perspective of spatial size and shape of input images.
- Our proposed method IN² is a successful example of introducing INR into the field of face inpainting.
- Our method sets new state-of-the-arts on the benchmark dataset CelebA-HQ [Karras *et al.*, 2017] in both ideal setting and real-world settings.

2 Related work

2.1 Image and Face Inpainting

Image inpainting has been a long-standing problem in low-level computer vision, with mainstream methods falling into two categories. The first is traditional, non-learning-based image inpainting, which relies on strong low-level assumptions. For example, images are considered to have strong auto-correlation which allows the masked area to be filled with adjacent pixels [Bertalmio *et al.*, 2003] or similar image patches [Barnes *et al.*, 2009]. However, these methods tend to fail when the damaged area is relatively large.

The second category is learning-based methods. With the boom in deep learning techniques, convolutional neural networks [Krizhevsky *et al.*, 2012], generative adversarial networks [Goodfellow *et al.*, 2014] and attention mechanism [Vaswani *et al.*, 2017] were successively proposed, which profoundly accelerates the development of inpainting. Many representative works [Yu *et al.*, 2018; Zeng *et al.*, 2019; Suvorov *et al.*, 2022] have been proposed, which can produce decent restoration content in the ideal setting (e.g., $512px \times 512px$). When it comes to face inpainting, diversified results and controllable editing have been successfully addressed as recent hot topics [Yildirim *et al.*, 2023]. However, it is far from meeting the real-world needs that various aspect ratios and high-resolution outputs are required.

2.2 Implicit Neural Representation

Implicit Neural Representation (INR) is a novel image representation that models an object as a function defined in a continuous domain, mapping location to signal value. By explicitly modeling signals with position information, the feature can express beyond resolution limitations. Moreover, from a practical perspective, INR is a coordinate-based MLP, which is a memory-efficient framework for high-resolution data. With these advantages, INR has shown outstanding potential in many fields. For example, NeRF [Martin-Brualla *et al.*, 2021] employs implicit neural representation to perform novel view synthesis, which maps coordinates to RGB colors for a specific scene. LIIF and its subsequent methods [Chen *et al.*, 2021; Cao *et al.*, 2023; Lee and Jin, 2022] propose a new solution for arbitrary super-resolution task by modeling an image as a function defined in a continuous domain. LINR [Xu and Jiao, 2023] explores the feasibility of INR in low-level vision domains such as inpainting. CoordFill [Liu *et al.*, 2023] can directly convert input into an INR representation by their hyper-network for inpainting. However, existing INR inpainting methods can not achieve decent performance

Methods	Reasons for constraints	Supported inputs
Deepfill	upsampling and downsampling in U-Net	evenly divided by 2^{num}
LAMA	upsampling and downsampling in U-Net	evenly divided by 2^{num}
MAT	window-based attention	square shape
CoordFill	patch-based supernetwork	square shape

Table 1: Existing methods only accept specific shape inputs.

in real-world face inpainting settings. We believe the potential of INR has not been fully explored yet.

3 Real-World Face Inpainting

In this section, we explore the performance of existing methods in real-world scenarios. Firstly, we define the real-world scenarios and introduce our test setting. Secondly, we apply existing methods in real-world face inpainting task, which results in a huge performance drop. In the third part, we introduce our efforts to improve existing methods by extra processing and retraining. Finally, we summarize all experiments and introduce our motivation.

We here specifically confine real-world scenarios in two aspects: aspect ratio and resolution. In terms of aspect ratio, we choose 3:4, 4:3 and 16:9 as representative ratios to conduct our experiments, for they are commonly used. As for resolution, under the condition of ensuring that the aspect ratio meets the requirements, we aim to make the resolution as close as possible to the original size of the images in the dataset to simulate the real-world demands in high-resolution scenarios. For example, to form our 16:9 (height: width) dataset, we crop the background area on both sides ($224px$ per side) of the image. It is worth emphasizing that the Lama in this paper was trained on $512px$ for fair evaluation purposes following [Suvorov *et al.*, 2022].

3.1 Apply Existing Face Inpainting Methods to Real-World Scenarios

Applying existing inpainting models to real-world scenarios, we find that existing methods have more or less limitations on the shape of the input image, as shown in Tab. 1. MAT [Li *et al.*, 2022] can only handle square input due to its window-based attention module, and CoordFill [Liu *et al.*, 2023] suffers the same limitation due to its patch-based hypernetwork architecture. Even the simplest conv-based methods require the resolution of the input to be an integer multiple of 2^{num} , where num is the number of layers in the U-Net, due to the downsample and upsample operations. We first consider the high-resolution inpainting task ($1024px \times 1024px$), where we can apply the existing model directly. As shown in Tab. 2, there is a huge performance drop between the ideal scenario ($512px \times 512px$) and the high-resolution scenario with the origin inference setting.

3.2 Adapt Existing Methods to Real-World Scenarios

We speculate that the performance degradation is due to the distortion of existing methods in understanding the structure of facial position when the input size changes. For the adaptation of existing face inpainting methods to real-world scenarios, we try to combine them with some extra resize processing. Specifically, we scale the input to the size of the

Methods	LaMa			MAT			CoordFill		
	Setting	512 × 512	1024 × 1024	512 × 512	1024 × 1024	512 × 512	1024 × 1024	512 × 512	1024 × 1024
Inference		origin	origin	resize	origin	origin	resize	origin	origin
PSNR↑		29.079	28.476	29.014	29.104	27.739	29.109	29.336	28.940
SSIM↑		0.913	0.912	0.915	0.914	0.908	0.914	0.893	0.910
LPIPS↓		0.064	0.089	0.0816	0.050	0.073	0.069	0.077	0.087

Table 2: Existing face inpainting models suffer from a performance drop in high-resolution scenarios and resizing can mitigate this problem. Compared with the performance between ideal and high-resolution setting in direct inference setting, we can see that models deteriorate severely in high-resolution scenarios. Compared with different inference settings, we can see that extra resize processing can improve the performance.

Setting	768 × 1024 (3:4)		1024 × 768 (4:3)		1024 × 576 (16:9)	
Inference	origin	resize	origin	resize	origin	resize
PSNR↑	29.073	29.445	29.095	29.449	29.942	30.026
SSIM↑	0.916	0.918	0.916	0.916	0.920	0.919
LPIPS↓	0.085	0.080	0.082	0.080	0.078	0.082

Table 3: Inference with extra resize processing tends to be a superior inference setting in most scenarios. We compared the performance of LaMa with and without additional processing in different aspect ratios and high-resolution settings. 'Resize' turns out to be a simple but effective way to improve the performance.

training data and scale the output back to its origin size (high-resolution) to mitigate the gap in spatial structure information between training data and testing data. As shown in Tab. 2, with extra resize processing, all methods can achieve superior performance in high-resolution scenario. we adopt extra resize processing in latter comparisons unless a specific explanation.

Intuitively, another method that can help existing methods maintain a decent understanding of facial structure and position in real-world scenarios is retraining them with arbitrary-shape input. We use images with different aspect ratios whose total size is close to $512px \times 512px$ as training data to fine-tune LaMa, dubbed retrain, which is the same training strategy as our method (discussed in section 4). We test the origin model and the retrained model in different settings without extra processing. As shown in Tab. 4, training with different aspect ratio data can not improve the robustness of LaMa in a real-world setting. Moreover, it causes a performance drop in the ideal setting, which indicates that the existing model design cannot support learning robust facial representations in shape-changing training data.

3.3 Summary and Motivation

So far, we now can output plausible content in real-world settings by extra resize processing in areas where position information is not sensitive (dubbed non-sensitive area), shown in Fig. 2 (d), which means we need to improve the capacity of modeling position for more realistic details. Moreover, we notice training with different aspect ratio images can not improve performance in total but can mitigate the duplicate artifact, especially around the eyes and nose, as shown in Fig. 2 (b) and (c), which means training model with arbitrary-shape input is not a way without prospect. Finally, as mentioned in [Xu *et al.*, 2021b], duplicate artifact in conv-based networks is caused by implicit and weak modeling method for position information. With all the above observations, we propose a position-aware model with the same training strategy.

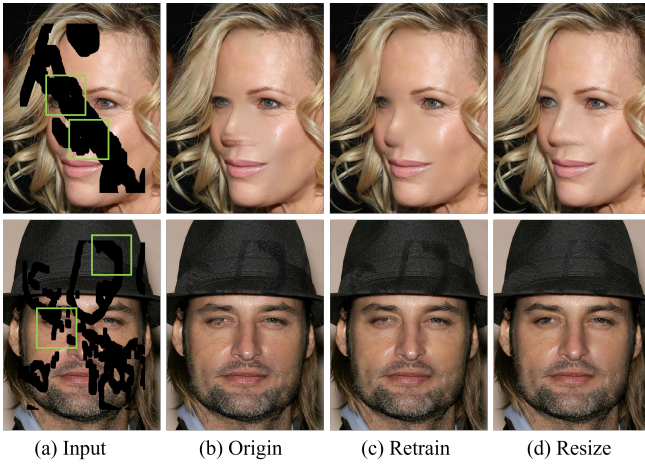


Figure 2: **Qualitative results of LaMa with various settings in a real-world setting** ($1024px \times 768px$). Original LaMa suffers a performance drop in a real-world setting, which can be improved by extra resize processing. However, it is still unsatisfactory in position-sensitive details, such as eyes and mouth.

Setting	512×512		1024×768 (4:3)		1024×576 (16:9)	
training	origin	retrain	origin	retrain	origin	retrain
PSNR \uparrow	29.079	28.677	29.095	28.832	29.942	29.819
SSIM \uparrow	0.913	0.909	0.916	29.104	0.920	0.920
LPIPS \downarrow	0.064	0.073	0.082	0.088	0.078	0.082

Table 4: **Although retrained with the arbitrary-shape dataset, the conv-based method still cannot adapt to real-world inpainting task.** We retrain LaMa with various aspect ratios data whose total number of pixels is equal to $512px \times 512px$, dubbed retrain. Compared with the origin model with resize processing, there is no obvious improvement.

4 Method

In this section, we first introduce the overview of our proposed Implicit Neural Inpainting Network (IN²), as shown in Fig. 3 (a). Then we illustrate the detailed design of each component. Finally, we discuss the training strategy and objective functions.

4.1 Overview

To address real-world face inpainting task, our model is required to accept arbitrary image shapes and efficiently get a precise understanding of the facial position structure. Specifically, A large receptive field, a feature processing module that does not restrict input, and powerful positional information modeling capabilities are characteristics that we need to consider in model design. In response to the above issues, we have carefully designed the following modules.

4.2 Implicit Neural Inpainting Network

Downsample Processing Encoder

The face inpainting task inherently requires a precise understanding of the facial structure to produce masked content, demanding a large effective receptive field. A cascade downsampling operation is a straightforward and popular solution [Nazeri *et al.*, 2019; Zeng *et al.*, 2022]. However, in the early encoding stage where the damaged area has not yet

been repaired, it is unreasonable to conduct the same down-sampling operation on both the damaged and intact areas. In practice, this may result in the information loss of intact areas and prevents the model from producing realistic detail for high-resolution applications. We propose a downsample processing block to alleviate this problem by providing additional feature processing in the early stage, which not only accelerates the restoration but also makes it easier for useful information in the features to be retained during the down-sampling process.

Specifically, we choose Fast Fourier Convolutions (FFC) as our basic module which allows us to use global context in early layers by the power of fast Fourier transform [Suvorov *et al.*, 2022]. As shown in Fig. 3 (b), we insert the FFC module behind the downsampling operation to retain more information. Moreover, we add a Channel Attention Block (CAB) to utilize global information. In practice, we stack three downsample processing blocks to form a downsample processing encoder that takes in the incomplete image concatenated with the given mask and produces features used for the later restoration.

Neighbor Hybrid Attention Blocks

More efficient feature processing modules can also bring better performance in face inpainting task [Li *et al.*, 2022]. However, the simple self-attention method [Vaswani *et al.*, 2017] is not efficient and the window-based attention [Liu *et al.*, 2021] method contradicts the arbitrary image shape demanded in real-world scenarios. To address this problem, we adopt the neighborhood attention block (NAB) [Hassani *et al.*, 2023] to avoid the restriction on resolution and process the feature efficiently. Additionally, inspired by previous works that convolution can help Transformer get preferable visual representation and achieve easier optimization [Wu *et al.*, 2021; Li *et al.*, 2023], we insert a Channel Attention Block (CAB) to aggregate global information, which is complementary to the local attention module. Following [Chen *et al.*, 2023], we multiply the output of CAB with a small constant α , to avoid the possible conflict of CAB and NAB on optimization and visual representation, the whole process is computed as

$$\begin{aligned}
 X_N &= \text{LN}(X), \\
 X_M &= \text{NAB}(X_N) + \alpha \text{CAB}(X_N), \\
 Y &= \text{MLP}(\text{LN}(X_M)) + X_M,
 \end{aligned} \tag{1}$$

where X_N and X_M denote the intermediate features. Y represents the output of the Neighbor Hybrid Attention Block (NHAB). We stack several NHAB to form an NHAB group for better capacity (as shown in Fig. 3 (c)).

Implicit Neural Pyramid Decoder

Position information is crucial for handling input images of different shapes in the real-world scenarios [Chen *et al.*, 2021]. We propose an implicit neural representation block to explicitly model position information and upsample feature compressed for a large receptive field, as shown in Fig. 3 (d). With the above module, we can establish a relationship between positional coordinates and features. Specifically, to predict the feature $\hat{a}(x_i)$ at an arbitrary query coordinate x_i ,

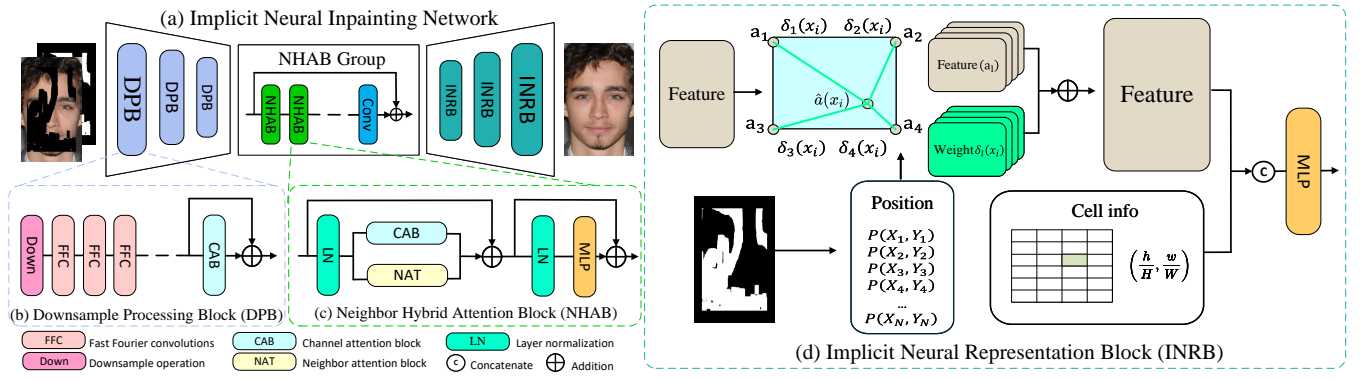


Figure 3: **The overview of the proposed implicit neural inpainting network for real-world face inpainting task.** (a) Implicit neural inpainting network consists of a downsample processing encoder, an attention body, and an implicit neural pyramid decoder. (b) We propose a downsample processing block to replace simple downsampling operation in other methods for more efficient encoding. (c) NHAB can overcome the limitation of window-based attention on image shape and enable superior facial structure learning. (d) Our implicit neural representation block can model position information explicitly for real-world task.

Settings	512 × 512			768 × 1024			1024 × 768			1024 × 576		
Metrics	PSNR↑	SSIM↑	LPIPS↓	PSNR↑	SSIM↑	LPIPS↓	PSNR↑	SSIM↑	LPIPS↓	PSNR↑	SSIM↑	LPIPS↓
Deepfill	26.677	0.898	0.109	28.507	0.917	0.097	29.742	0.916	0.083	29.084	0.918	0.100
LAMA	29.079	0.913	0.064	29.445	0.918	0.080	29.448	0.915	0.080	30.026	0.918	0.082
MAT	29.104	0.914	0.050	29.392	0.916	0.068	30.001	0.923	0.066	29.743	0.917	0.069
CoordFill	29.336	0.893	0.077	29.801	0.919	0.083	29.209	0.913	0.067	29.743	0.917	0.086
IN ² (Ours)	30.285	0.927	0.044	30.391	0.924	0.056	30.040	0.919	0.061	31.597	0.929	0.051

Table 5: **Quantitative results in different settings.** We achieve superior performance in both ideal settings and real-world settings.

We gather its neighborhood information. The entire process is computed as

$$\hat{a}(x_i) = \sum_l f(a_l, \delta_l(x_i)), \quad (2)$$

where l is the point index in the local region centered at the query coordinate x_i , (l can be top-left, top-right, bottom-left and bottom-right), and $\delta_l(x_i)$ is the weight of the neighboring feature value a_l . $\delta_l(x_i)$ is the distance between x_i and the position of a_l . The feature is upsampled during the above process. Moreover, to adapt to various image shapes better, we introduce the cell information which specifies the height and width of the query pixel [Chen *et al.*, 2021], which is defined as

$$(c_h, c_w) = \left(\frac{h}{H}, \frac{w}{W} \right), \quad (3)$$

where h, w represents the height and width of the feature, and H, W represents the height and width of output respectively.

However, the gap between the high-resolution output demanded by real-world downstream applications and the low-resolution feature required for a large receptive field is not negligible. One-step upsampling is not an appropriate solution, which leads to a decrease in model performance [Fu *et al.*, 2019]. In light of this, we propose an implicit neural pyramid decoder to produce filled images progressively. Specifically, we set up a three-layer pyramid, where each layer is an INRB module that operates on its resolution and only the final layer operates on the target one. The whole process is computed as

$$a_{\text{layer}+1}(x_i) = \text{MLP}(\hat{a}_{\text{layer}}(x_i), (c_h, c_w)), \quad (4)$$

where $a_{\text{layer}+1}(x_i)$ is feature value at the coordinate x_i in the pyramid, layer indicates which layer of the pyramid the feature belongs to and (c_h, c_w) are the cell information, which specifies the height and width of the query pixel.

4.3 Training Details

Adaptive Training Strategy

We want to train models on data with different aspect ratios to achieve robust facial structure modeling capabilities. Specifically, we randomly crop the marginal area to create datasets with different aspect ratios while maintaining the total pixels of each image is close to $512px \times 512px$. Compared to the result in Tab. 4, Our model design enables it to learn robust facial structure modeling ability on data with drastic changes in spatial positional information. The ablation study validates that our strategy is simple and effective.

Training Objective

We follow CoordFill [Liu *et al.*, 2023] to train our model with different perception losses, including saturating adversarial loss [Goodfellow *et al.*, 2014], perceptual loss [Johnson *et al.*, 2016] and feature matching loss [Wang *et al.*, 2018]. Besides, we also use the R_1 regularization [Mescheder *et al.*, 2018], written as $R_1 = E_x \|\nabla D(x)\|$, to stabilize the training. We calculate the adversarial loss as

$$\mathcal{L}_G = -E_{\hat{x}} [\log(D(\hat{x}))], \quad (5)$$

$$\mathcal{L}_D = -E_x [\log(D(x))] - E_{\hat{x}} [\log(1 - D(\hat{x}))], \quad (6)$$

where x and \hat{x} are the real and generated images. The perceptual loss is formulated as

$$\mathcal{L}_{per} = \sum_i \tau \|\phi_i(\hat{x}) - \phi_i(x)\|_1, \quad (7)$$



Figure 4: **Qualitative comparison with different aspect ratios.** We display zoom-in results for easier comparison of position-sensitive details and whole results can be found in the appendix.

where $\phi_i(\cdot)$ denotes the layer activation of a pre-trained VGG-19 [Simonyan and Zisserman, 2014] network. τ calculates the differences in the feature domain via L_1 loss. Next, the feature matching loss is adopted for stabilizing the GAN training [Liu *et al.*, 2023; Suvorov *et al.*, 2022] and can be formulated as

$$L_{fm} = \sum_i \tau(D^i(x), D^i(\hat{x})), \quad (8)$$

where D^i denotes the activations from the i -th layer of the discriminator D . The overall loss of the generator is

$$L_{total} = L_G + \lambda_{per} L_{per} + \lambda_{fm} L_{fm} + \lambda_R R_1. \quad (9)$$

where $\lambda_{per} = 10$, $\lambda_{fm} = 0.1$ and $\lambda_R = 10$.

5 Experiments

In this section, implementation details, dataset and evaluation metrics are first introduced. Then we conduct qualitative and quantitative comparative experiments with SOTA methods in both ideal and real-world scenarios. Additionally, we compare our method with existing methods with super-resolution networks as post-processing, as it is an intuitive solution that can handle real-world scenarios. Moreover, we introduce an

ablation study. Due to limited layout, latency and model size information can be found in the appendix.

5.1 Implementation Details

All experiments are carried out on 2 NVIDIA RTX 4090 GPUs. All models are trained for 100 epochs with batch size 3, and the learning rate decays by cosine annealing after a warm-up phase of 15 epochs. We use the Adam [Kingma and Ba, 2014] optimizer with an initial learning rate 4×10^{-5} and the maximum 4×10^{-4} .

In our framework, the number of the pyramid layer is three and the convolution channel dimensions for the encoder and decoder are 256, 128, and 64, respectively. The attention body contains two neighbor hybrid attention groups. For each of them, there are four neighbor hybrid attention blocks. Empirically, we set the α as a small constant number (0.03) following [Chen *et al.*, 2023].

5.2 Datasets and Metrics

We experiment on the CelebA-HQ [Karras *et al.*, 2017] dataset. We use the free-form masks [Liu *et al.*, 2018] for training and testing, while the masked area is 20% – 30% following common settings [Suvorov *et al.*, 2022; Liu *et al.*, 2023].

Settings	(a)Real-world (1024×576)		(b)High-resolution (1024×1024)	
Model	MAT+LIIF	IN ²	MAT+GFPGAN	IN ²
PSNR \uparrow	29.531	31.496	28.758	29.683
SSIM \uparrow	0.914	0.936	0.910	0.929
LPIPS \downarrow	0.070	0.052	0.085	0.062

Table 6: **Comparisons with SR-based Post-Processing.** We compare our IN² with SOTA inpainting model plus the super-resolution model in real-world and high-resolution settings respectively. The results indicate our method has better performance.

As for metrics, we follow previous works [Suvorov *et al.*, 2022; Liu *et al.*, 2023] to use PSNR, SSIM [Wang *et al.*, 2004] and LPIPS [Zhang *et al.*, 2018], because they can evaluate images from different perspectives.

5.3 Comparison with SOTAs

We compare the performance of our method and other SOTA methods under different aspect ratios of input in both high-resolution and low-resolution scenarios. For a fair comparison, we use publicly available model weights to test on the same masks, except for LaMa. Because the public weight is trained on $256px \times 256px$, we train it on $512px \times 512px$ for comparison. It is worth emphasizing that all comparison methods, except for LaMa, adopt extra processing to meet the requirements of the model and enhance performance under non-1:1 aspect ratio. When the resolution of the test set is close to $512px$, LaMa do not need extra processing. Due to layout limitations, we only present the results of ideal scenario and high-resolution scenarios with different aspect ratios here. More results (e.g., low-resolution with different aspect ratios) can be found in the appendix.

Quantitative Comparisons

For the settings in previous work [Suvorov *et al.*, 2022] (dubbed ideal setting), we conduct the experiments at $512px \times 512px$. As for real-world settings, we conduct experiments in three representative aspect ratios with high-resolution format, including $768px \times 1024px$, $1024px \times 768px$, and $1024px \times 576px$. As illustrated in Tab. 5, no matter the ideal setting and real-world settings, our method achieves state-of-the-art performance. More experimental results are provided in the appendix.

Qualitative Comparisons

We show the qualitative inpainting results in real-world scenarios (different aspect ratios in high-resolution format) in Fig. 4. To focus on the position-sensitive details, where existing methods fail, such as eyes and mouth, we post the zoom-in results. The whole image results are provided in the appendix. Compared with other methods, our method achieves superior performance in all settings.

5.4 Comparisons with SR-based Post-Processing

A simple and straight alternative to our method is to resize the input to comply with the training data and use a super-resolution model to scale the inpainting output back to its original size. We conduct this comparison in the real-world ($1024px \times 576px$) and high-resolution settings ($1024px \times 1024px$) respectively. For a fair comparison, we choose MAT [Li *et al.*, 2022] (CVPR 22 best paper finalist)

Adaptive Training Strategy	DBP	NHAB	Pyramid	PSNR \uparrow	SSIM \uparrow	LPIPS \downarrow
				29.690	0.916	0.074
✓				31.174	0.926	0.063
✓	✓			31.321	0.928	0.059
✓	✓	✓		31.363	0.935	0.055
✓	✓	✓	✓	31.496	0.936	0.052

Table 7: **Ablation experiments.** As we insert the module we design, the performance of the model is constantly improving, which indicates the effectiveness of our proposed module.

as the inpainting backbone for its excellent performance. We choose LIIF [Chen *et al.*, 2021] (arbitrary SR model) for real-world setting and GFPGAN [Wang *et al.*, 2021] (human face SR model) for high-resolution setting. As shown in Tab.6 (a) and (b), our method has better performance because we internalize the position modeling ability of INR into the inpainting network. Although the extra SR network can improve the resolution, it cannot preserve the original image texture, which results in bad evaluation scores.

5.5 Ablation Study

In this section, we tease apart components in our framework and evaluate them in a real-world scenario ($1024px \times 576px$). The quantitative comparison is shown in Tab. 7. Specifically, we replace the adaptive training strategy with normal training data ($512px \times 512px$). We use the encoder of LAMA[Suvorov *et al.*, 2022] to replace DPB and increase its parameters for fair comparison and set the layer number of the pyramid to 1 to validate the effectiveness of our pyramid. As for the attention module, we substitute it with more FFC modules, which is a common choice in networks designed without attention mechanisms [Suvorov *et al.*, 2022; Jain *et al.*, 2023]. The results demonstrate that our proposed modules can improve the receptive field, semantic learning and enhance the model’s generalization respectively, which is further beneficial for the overall performance.

According to the results of the ablation experiment, part of the improvements in our model come from the training strategy. It is worth emphasizing that without our INR structure, the model cannot learn robust inpainting capacity under the same training strategy, as shown in Tab. 4.

6 Conclusion

In this paper, we focus on real-world face inpainting task (e.g., high-resolution and arbitrary aspect ratio) and find that existing methods have significant shortcomings in terms of both acceptable inputs and performance in real-world scenarios. Targeting the task characteristics that require a precise understanding of the facial position structure, we try to adapt existing methods to real-world scenarios with extra resize processing and retraining. However these methods still fail to achieve satisfactory results due to their limited ability to model position information. To address this issue, we propose an implicit neural network (IN²). With our well-designed modules, it can explicitly model facial position structure and accept arbitrary-size input in real-world face inpainting scenarios. Our experiments show the robust performance of the proposed method in several real-world settings compared with several state-of-the-art methods.

A Overview

In this appendix, we supplement a comparison of extra processing methods and a comparative experiment in different real-world settings. Moreover, we add the whole image corresponding to the zoom-in results in the main text. Finally, we list the latency and model size comparison.

B Comparison of Extra Processing Methods

For SOTA methods that require square input (e.g., MAT), we test another extra processing method. We scale the long edge of the input to $512px$ and then perform padding operations, dubbed pad. Moreover, we try different pad methods, including constant pad and edge pad. We compare pad and the resize processing in the main text in real-world setting with a relative low-resolution format ($683px \times 384px$), as shown in Tab. 8. Extra resize processing tends to be better choice, and we adopt this method for fair comparison.

Inference Settings	pad-constant	pad-edge	resize
PSNR \uparrow	29.448	29.715	29.991
SSIM \uparrow	0.908	0.910	0.919
LPIPS \downarrow	0.067	0.065	0.060

Table 8: **Comparison of extra processing methods.** Extra resize processing tends to be better.

C Quantitative Comparisons in More Settings

We conduct comparative experiments between our method and the main state-of-the-art methods under multiple settings, including the pure high-resolution setting ($1024px \times 1024px$) and low-resolution settings with various aspect ratios. As for the low-resolution settings, we keep the total number of pixels in the image equal to 512×512 while keeping the aspect ratio of the input constantly changing, which helps us see the impact on model performance when the aspect ratio changes. As shown in Table. 10, our method achieves better performance in all settings.

D More Visual Results

To better demonstrate the inpainting performance in details where are sensitive to the change of position information, such as eyes and nose, we only post the zoom-in results in the main paper. We supplement some whole results in this section. To make it easier to compare the differences between different methods, we only list part of methods that achieve better performance.

Methods	LaMa	MAT	CoordFill	IN^2 (Ours)
Param	27.3 M	61.6M	31.6M	15.5M
Latency	13ms	28ms	10ms	20ms

Table 9: **Model size and the inference time.** We test inference time at $512px \times 512px$ in RTX 4090

E Model Size and Latency

We test the inference time of mentioned SOTA methods and our method at $512px \times 512px$ in RTX 4090 and add the model information, as shown in Table 2. At similar inference speeds, our model has fewer parameters. Due to the bottleneck of our computing speed being attention operations, our inference time can be shorter in the future.

References

- [Barnes *et al.*, 2009] Connelly Barnes, Eli Shechtman, Adam Finkelstein, and Dan B Goldman. PatchMatch: A randomized correspondence algorithm for structural image editing. *TOG*, 28(3):24, 2009.
- [Bertalmio *et al.*, 2003] Marcelo Bertalmio, Luminia Vese, Guillermo Sapiro, and Stanley Osher. Simultaneous structure and texture image inpainting. *TIP*, 12(8):882–889, 2003.
- [Cao *et al.*, 2023] Jiezhong Cao, Qin Wang, Yongqin Xian, Yawei Li, Bingbing Ni, Zhiming Pi, Kai Zhang, Yulun Zhang, Radu Timofte, and Luc Van Gool. CioSR: Continuous implicit attention-in-attention network for arbitrary-scale image super-resolution. In *CVPR*, 2023.
- [Chen *et al.*, 2021] Yinbo Chen, Sifei Liu, and Xiaolong Wang. Learning continuous image representation with local implicit image function. In *CVPR*, pages 8628–8638, 2021.
- [Chen *et al.*, 2023] Xiangyu Chen, Xintao Wang, Jiantao Zhou, Yu Qiao, and Chao Dong. Activating more pixels in image super-resolution transformer. In *CVPR*, pages 22367–22377, June 2023.
- [Fu *et al.*, 2019] Zhichao Fu, Yu Kong, Yingbin Zheng, Hao Ye, Wenxin Hu, Jing Yang, and Liang He. Cascaded detail-preserving networks for super-resolution of document images. In *ICDAR*, pages 240–245, 2019.
- [Goodfellow *et al.*, 2014] Ian Goodfellow, Jean Pouget-Abadie, Mehdi Mirza, Bing Xu, David Warde-Farley, Sherjil Ozair, Aaron Courville, and Yoshua Bengio. Generative adversarial nets. *NeurIPS*, 27, 2014.
- [Hassani *et al.*, 2023] Ali Hassani, Steven Walton, Jiachen Li, Shen Li, and Humphrey Shi. Neighborhood attention transformer. In *CVPR*, pages 6185–6194, 2023.
- [Jain *et al.*, 2023] Jitesh Jain, Yuqian Zhou, Ning Yu, and Humphrey Shi. Keys to Better Image Inpainting: Structure and texture go hand in hand. In *WACV*, pages 208–217, 2023.
- [Johnson *et al.*, 2016] Justin Johnson, Alexandre Alahi, and Li Fei-Fei. Perceptual losses for real-time style transfer and super-resolution. In *ECCV*, pages 694–711, 2016.
- [Karras *et al.*, 2017] Tero Karras, Timo Aila, Samuli Laine, and Jaakko Lehtinen. Progressive growing of gans for improved quality, stability, and variation. *arXiv preprint arXiv:1710.10196*, 2017.
- [Kingma and Ba, 2014] Diederik P Kingma and Jimmy Ba. Adam: A method for stochastic optimization. *arXiv preprint arXiv:1412.6980*, 2014.

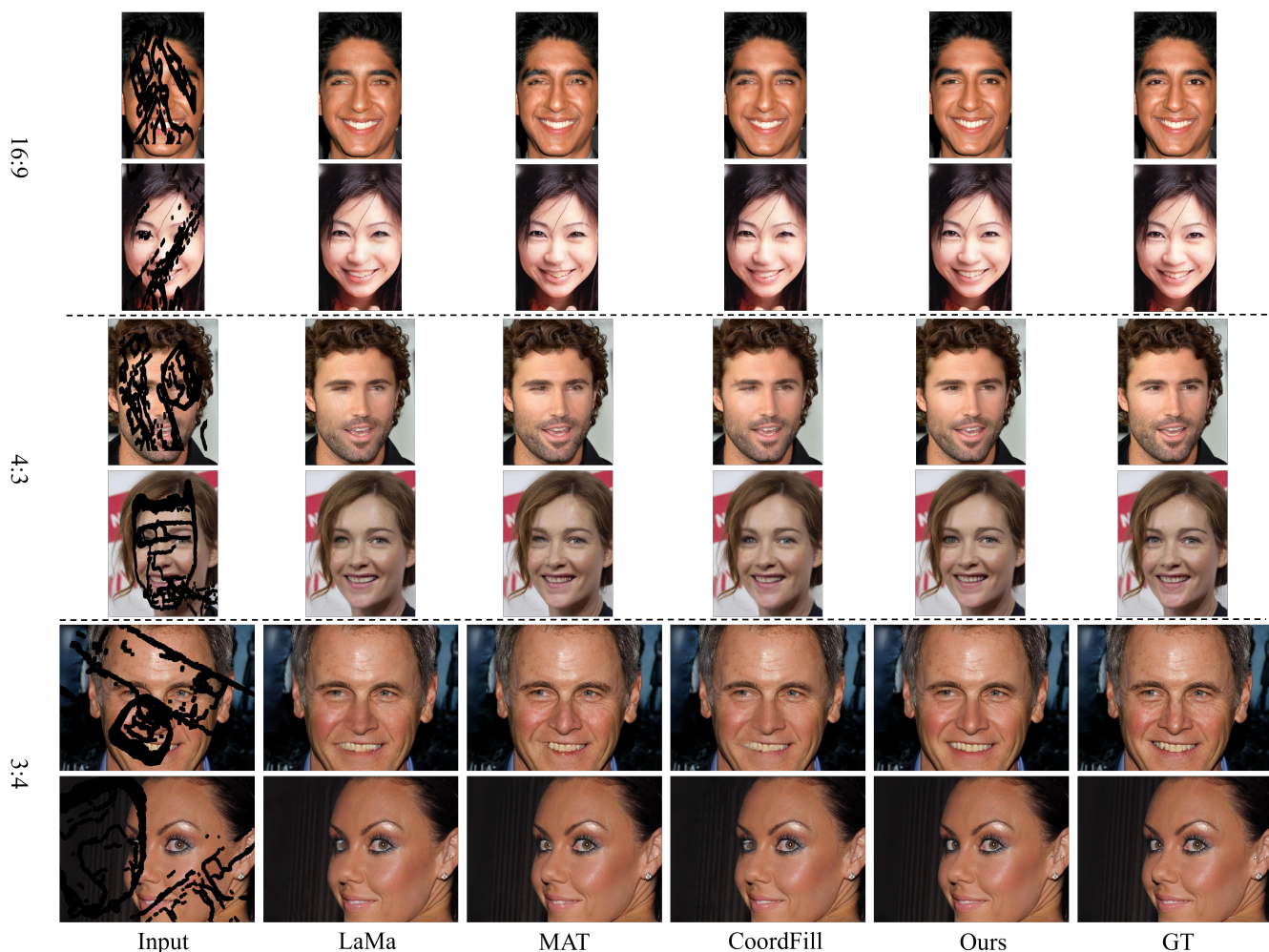


Figure 5: **Qualitative comparison with different aspect ratios.**

- [Krizhevsky *et al.*, 2012] Alex Krizhevsky, Ilya Sutskever, and Geoffrey E Hinton. Imagenet classification with deep convolutional neural networks. *NeurIPS*, 25, 2012.
- [Lee and Jin, 2022] Jaewon Lee and Kyong Hwan Jin. Local texture estimator for implicit representation function. In *CVPR*, pages 1929–1938, June 2022.
- [Li *et al.*, 2022] Wenbo Li, Zhe Lin, Kun Zhou, Lu Qi, Yi Wang, and Jiaya Jia. MAT: Mask-aware transformer for large hole image inpainting. In *CVPR*, pages 10758–10768, 2022.
- [Li *et al.*, 2023] Kunchang Li, Yali Wang, Junhao Zhang, Peng Gao, Guanglu Song, Yu Liu, Hongsheng Li, and Yu Qiao. UniFormer: Unifying convolution and self-attention for visual recognition. *TPAMI*, pages 1–18, 2023.
- [Liu *et al.*, 2018] Guilin Liu, Fitsum A Reda, Kevin J Shih, Ting-Chun Wang, Andrew Tao, and Bryan Catanzaro. Image inpainting for irregular holes using partial convolutions. In *ECCV*, pages 85–100, 2018.
- [Liu *et al.*, 2021] Ze Liu, Yutong Lin, Yue Cao, Han Hu, Yixuan Wei, Zheng Zhang, Stephen Lin, and Baining Guo. Swin transformer: Hierarchical vision transformer using shifted windows. In *ICCV*, pages 10012–10022, 2021.
- [Liu *et al.*, 2023] Weihuang Liu, Xiaodong Cun, Chi-Man Pun, Menghan Xia, Yong Zhang, and Jue Wang. Coord-Fill: Efficient high-resolution image inpainting parameterized coordinate querying. In *AAAI*, pages 1746–1754, 2023.
- [Martin-Brualla *et al.*, 2021] Ricardo Martin-Brualla, Noha Radwan, Mehdi SM Sajjadi, Jonathan T Barron, Alexey Dosovitskiy, and Daniel Duckworth. Nerf in the Wild: Neural radiance fields for unconstrained photo collections. In *CVPR*, pages 7210–7219, 2021.
- [Mescheder *et al.*, 2018] Lars Mescheder, Andreas Geiger, and Sebastian Nowozin. Which training methods for gans do actually converge? In *ICML*, pages 3481–3490. PMLR, 2018.
- [Nazeri *et al.*, 2019] Kamyar Nazeri, Eric Ng, Tony Joseph, Faisal Qureshi, and Mehran Ebrahimi. EdgeConnect: Structure guided image inpainting using edge prediction. In *CVPR*, pages 3265–3274, 2019.

Methods	1024 × 1024			443 × 591			591 × 443			683 × 384		
	PSNR↑	SSIM↑	LPIPS↓	PSNR↑	SSIM↑	LPIPS↓	PSNR↑	SSIM↑	LPIPS↓	PSNR↑	SSIM↑	LPIPS↓
LAMA	29.014	0.915	0.082	29.516	0.915	0.065	29.463	0.913	0.064	30.330	0.920	0.063
MAT	29.109	0.914	0.069	29.634	0.918	0.056	29.454	0.916	0.056	29.991	0.919	0.060
CoordFill	28.962	0.911	0.087	29.624	0.916	0.074	29.579	0.914	0.074	29.978	0.917	0.082
IN^2 (Ours)	29.683	0.929	0.062	30.508	0.928	0.045	30.124	0.921	0.047	31.864	0.935	0.051

Table 10: **Quantitative results in different settings.** We achieve superior performance in all settings.

- [Simonyan and Zisserman, 2014] Karen Simonyan and Andrew Zisserman. Very deep convolutional networks for large-scale image recognition. *arXiv preprint arXiv:1409.1556*, 2014.
- [Suvorov *et al.*, 2022] Roman Suvorov, Elizaveta Logacheva, Anton Mashikhin, Anastasia Remizova, Arsenii Ashukha, Aleksei Silvestrov, Naejin Kong, Harshith Goka, Kiwoong Park, and Victor Lempitsky. Resolution-robust large mask inpainting with fourier convolutions. In *WACV*, pages 2149–2159, 2022.
- [Vaswani *et al.*, 2017] Ashish Vaswani, Noam Shazeer, Niki Parmar, Jakob Uszkoreit, Llion Jones, Aidan N Gomez, Łukasz Kaiser, and Illia Polosukhin. Attention is all you need. *NeurIPS*, 30, 2017.
- [Wang *et al.*, 2004] Zhou Wang, Alan C Bovik, Hamid R Sheikh, and Eero P Simoncelli. Image quality assessment: from error visibility to structural similarity. *TIP*, 13(4):600–612, 2004.
- [Wang *et al.*, 2018] Ting-Chun Wang, Ming-Yu Liu, Jun-Yan Zhu, Andrew Tao, Jan Kautz, and Bryan Catanzaro. High-resolution image synthesis and semantic manipulation with conditional gans. In *CVPR*, pages 8798–8807, 2018.
- [Wang *et al.*, 2021] Xintao Wang, Yu Li, Honglun Zhang, and Ying Shan. Towards real-world blind face restoration with generative facial prior. In *CVPR*, pages 9168–9178, 2021.
- [Wu *et al.*, 2021] Haiping Wu, Bin Xiao, Noel Codella, Mengchen Liu, Xiyang Dai, Lu Yuan, and Lei Zhang. CvT: Introducing convolutions to vision transformers. In *ICCV*, pages 22–31, 2021.
- [Xu and Jiao, 2023] Wentian Xu and Jianbo Jiao. Revisiting implicit neural representations in low-level vision. In *ICLR*, 2023.
- [Xu *et al.*, 2021a] Rui Xu, Minghao Guo, Jiaqi Wang, Xiaoxiao Li, Bolei Zhou, and Chen Change Loy. Texture memory-augmented deep patch-based image inpainting. *TIP*, 30:9112–9124, 2021.
- [Xu *et al.*, 2021b] Rui Xu, Xintao Wang, Kai Chen, Bolei Zhou, and Chen Change Loy. Positional encoding as spatial inductive bias in gans. In *CVPR*, pages 13569–13578, 2021.
- [Yildirim *et al.*, 2023] Ahmet Burak Yildirim, Hamza Pehlivan, Bahri Batuhan Bilecen, and Aysegul Dundar. Diverse inpainting and editing with gan inversion. In *CVPR*, pages 23120–23130, 2023.
- [Yu *et al.*, 2018] Jiahui Yu, Zhe Lin, Jimei Yang, Xiaohui Shen, Xin Lu, and Thomas S Huang. Generative image inpainting with contextual attention. In *CVPR*, pages 5505–5514, 2018.
- [Zeng *et al.*, 2019] Yanhong Zeng, Jianlong Fu, Hongyang Chao, and Baining Guo. Learning pyramid-context encoder network for high-quality image inpainting. In *CVPR*, pages 1486–1494, 2019.
- [Zeng *et al.*, 2022] Yanhong Zeng, Jianlong Fu, Hongyang Chao, and Baining Guo. Aggregated contextual transformations for high-resolution image inpainting. *TVCG*, pages 3266–3280, 2022.
- [Zhang *et al.*, 2018] Richard Zhang, Phillip Isola, Alexei A Efros, Eli Shechtman, and Oliver Wang. The unreasonable effectiveness of deep features as a perceptual metric. In *CVPR*, pages 586–595, 2018.